Stochastic Environmental Research and Risk Assessment 15 (2001) 33–46 © Springer-Verlag 2001

Dissolution of nonaqueous phase liquid pools in anisotropic aquifers

E. T. Vogler, C. V. Chrysikopoulos

Abstract. A two-dimensional numerical transport model is developed to determine the effect of aquifer anisotropy and heterogeneity on mass transfer from a dense nonaqueous phase liquid (DNAPL) pool. The appropriate steady state groundwater flow equation is solved implicitly whereas the equation describing the transport of a sorbing contaminant in a confined aquifer is solved by the alternating direction implicit method. Statistical anisotropy in the aquifer is introduced by two-dimensional, random log-normal hydraulic conductivity field realizations with different directional correlation lengths. Model simulations indicate that DNAPL pool dissolution is enhanced by increasing the mean log-transformed hydraulic conductivity, groundwater flow velocity, and/or anisotropy ratio. The variance of the log-transformed hydraulic conductivity distribution is shown to be inversely proportional to the average mass transfer coefficient.

1 Introduction

The dissolution of dense nonaqueous phase liquids (DNAPLs) in subsurface environments is a long lasting process that results in groundwater quality degredation. Furthermore, DNAPLs may remain in aquifers for long periods of time due to their low aqueous solubilities. DNAPL pools are often formed atop low permeability layers and in aquifers with even subtle heterogeneity (Khachikian and Harmon, 2000). The majority of existing literature on contaminant transport resulting from DNAPL pool dissolution is associated with homogeneous aquifers (Johnson and Pankow, 1992; Whelan et al., 1994; Chrysikopoulos, 1995a; Lee and Chrysikopoulos, 1995; Mason and Kueper, 1996; Kim and Chrysikopoulos, 1999; and Tatalovich et al., 2000, to mention a few). The incorporation of the spatial variability of soil and hydraulic properties in the study of fluid flow and solute transport can be achieved only by means of stochastic models (Christakos, 1992). All properties which affect the rates of groundwater flow and transport have been shown to be highly spatially variable (Chrysikopoulos, 1995b). Consequently, such variabilities may significantly influence DNAPL pool formation (Freeze, 1975; Sudicky, 1986; Burr et al., 1994; Russo et al., 1994; Manivannan et al., 1996) as well as the complex behavior of DNAPL dissolution (Rivett et al., 1994).

E. T. Vogler, C. V. Chrysikopoulos (✉)
Department of Civil and Environmental Engineering,
University of California, Irvine, CA 92697, USA
e-mail: costas@eng.uci.edu

Numerous studies have focused on DNAPL dissolution in porous media. Powers et al. (1998) identified the importance of transverse dispersion and flow bypassing on the dissolution of NAPLs entrapped in a coarse sand lens as a function of NAPL saturation, and demonstrated that the local equilibrium assumption is appropriate for the majority of the dissolution duration period, especially when the NAPL saturation is greater than 15%. Mayer and Miller (1996) performed two-dimensional numerical multi-phase flow, NAPL emplacement, and NAPL dissolution simulations, and have shown that aquifer properties affect the spatial distribution of residual NAPLs, and the variance of the log-normal intrinsic permeability contributes more to mass elution rates than the horizontal correlation length scale. Lee and Chrysikopoulos (1998) have determined that the average mass flux originating from the dissolution of a well defined DNAPL pool is smaller within a statistically anisotropic confined aquifer than a homogeneous aquifer, whereas the spreading of dissolved contaminants is greater in a statistically anisotropic aquifer. It should be noted however, that a thorough investigation of the effects of aquifer anisotropy on DNAPL pool dissolution and associated overall mass transfer coefficient has yet to be conducted.

For the work presented here, a two-dimensional numerical model is developed to determine the effect of aquifer anisotropy on the average mass transfer coefficient of a 1,1,2-trichloroethane (1,1,2-TCA) DNAPL pool formed on bedrock in a statistically anisotropic confined aquifer. Statistical anisotropy in the aquifer is introduced by representing the spatially variable hydraulic conductivity as a log-normally distributed random field described by an anisotropic exponential covariance function.

2
Model development

2.1
Contaminant transport

The transport of a sorbing contaminant in two-dimensional, heterogeneous, saturated porous media, resulting from the dissolution of a single component DNAPL pool, is described by the following partial differential equation:

$$R\frac{\partial C(t,x,z)}{\partial t} = \frac{\partial}{\partial x}\left[D_x(x,z)\frac{\partial C(t,x,z)}{\partial x}\right] + \frac{\partial}{\partial z}\left[D_z(x,z)\frac{\partial C(t,x,z)}{\partial z}\right] - \frac{\partial}{\partial x}[U_x(x,z)C(t,x,z)] - \frac{\partial}{\partial z}[U_z(x,z)C(t,x,z)] \quad , \tag{1}$$

where R is the retardation; $C(t,x,z)$ is the aqueous contaminant concentration; t is time; x, z are the spatial coordinates in the longitudinal and vertical directions, respectively; D_x, D_z are the longitudinal and vertical hydrodynamic dispersion coefficients, respectively; and U_x, U_z are the longitudinal and vertical interstitial fluid velocities, respectively.

Dissolution of a DNAPL pool results in the development of a concentration boundary layer above the DNAPL-water interface. Assuming that the thickness of the NAPL pool is insignificant relative to the thickness of the aquifer, the contaminant mass transfer from a DNAPL-water interface is then described by the following relationship (Chrysikopoulos et al., 1994);

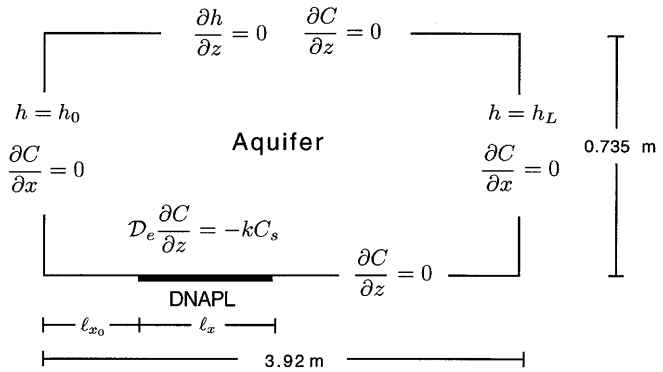

Fig. 1. Schematic illustration of the aquifer domain and DNAPL pool location together with the appropriate boundary conditions employed

$$-\mathscr{D}_e \frac{\partial C(t,x,0)}{\partial z} = k(t,x)[C_s - C(t,x,+\infty)] \quad \ell_{x_0} < x < \ell_{x_0} + \ell_x \ , \tag{2}$$

where $\mathscr{D}_e = \mathscr{D}/\tau^*$ is the effective diffusion coefficient ($\mathscr{D}$ is the molecular diffusion coefficient and $\tau^* \geq 1$ is the tortuosity of the porous medium); $k(t,x)$ is the local mass transfer coefficient; C_s is the aqueous solubility concentration of the contaminant; $C(t,x,+\infty)$ is the background aqueous contaminant concentration above the concentration boundary layer; ℓ_{x_0} is the location of the origin of the NAPL pool; and ℓ_x is the length of the NAPL pool. A definition sketch is provided in Fig. 1. The left-hand side term in (2) describes the diffusive flux into the boundary layer at the DNAPL-water interface, given by Fick's law, and the right-hand side describes the advective mass flux.

The thickness of the boundary layer that results from a dissolving DNAPL pool depends upon the hydrodynamics of the porous medium. Boundary layer thickness is defined as the height above the DNAPL-water interface for which $[C(t,x,0) - C(t,x,z)]/[C(t,x,0) - C(t,x,\infty)] = 0.99$ (Incropera and DeWitt, 1990, p. 321). For increasing interstitial groundwater velocities the boundary layer becomes progressively thinner. A thin boundary layer corresponds to steeper concentration gradients and the greater the concentration gradient the greater the mass transfer of the dissolving DNAPL. Consequently, the local mass transfer coefficient decreases with distance from the front end of the DNAPL pool, and has a maximum value at the leading or upstream edge. At early time the mass transfer coefficient is temporally dependent; however, at steady-state physicochemical and hydrodynamic conditions it becomes independent of time (Chrysikopoulos and Lee, 1998).

The appropriate initial and boundary conditions for a DNAPL pool formed above an impermeable stratum at the bottom of a confined aquifer are

$$C(0,x,z) = 0 \ , \tag{3}$$

$$\frac{\partial C(t,0,z)}{\partial x} = \frac{\partial C(t,L,z)}{\partial x} = 0 \ , \tag{4}$$

$$\mathscr{D}_e \frac{\partial C(t,x,0^+)}{\partial z} = -k(t,x)C_s \quad \ell_{x_0} < x < \ell_{x_0} + \ell_x \ , \tag{5}$$

and

$$\frac{\partial C(t,x,H)}{\partial z} = 0 \quad , \tag{6}$$

where L is the length of the aquifer, and H is the height of the aquifer. The condition (3) establishes that there is no initial dissolved NAPL within the two-dimensional porous medium. The boundary condition (4) preserves concentration continuity for a finite system. The boundary condition (5) describes the mass flux from the DNAPL-water interface. Boundary condition (6) represents a zero dispersive flux and implies that the aquifer is confined by an impermeable layer at height H.

2.2 Groundwater flow

In this study the NAPL phase is considered immobile; consequently, aquifer anisotropy is governed by the variability in the hydraulic conductivity field. The porous medium is also assumed to be fully saturated, making the hydraulic conductivity time invariant. The two-dimensional hydraulic conductivity field is generated stochastically by using the computer program SPRT2D (Gutjhar, 1989). It is assumed that the hydraulic conductivity follows a log-normal distribution and the log-transformed hydraulic conductivity, Y, varies spatially according to the following anisotropic exponential covariance function (Gelhar and Axness, 1983; Sudicky, 1986; Russo et al., 1994; Lee and Chrysikopoulos, 1998).

$$C_Y(\mathbf{r}) = \sigma_Y^2 \exp\left[-\left(\frac{r_x^2}{\zeta_x^2} + \frac{r_z^2}{\zeta_z^2}\right)^{1/2}\right] \quad , \tag{7}$$

where $\mathbf{r} = (r_x, r_z)^{\mathrm{T}}$ is a two-dimensional vector whose magnitude is the separation distance of two hydraulic conductivity measurements; ζ_x and ζ_z are the correlation length scales in the x and z directions, respectively; and σ_Y^2 is the variance of the log-transformed hydraulic conductivity defined as

$$Y = \ln K \quad , \tag{8}$$

where K is the hydraulic conductivity. The stochastic realizations of $K(x,z)$ are locally independent of direction. Anisotropy is therefore introduced globally by the overall spatial variability of the hydraulic conductivity field (Burr et al., 1994). Log-transformed hydraulic conductivity fields were created for the model aquifer illustrated in Fig. 1 with length $L = 3.92$ m and height $H = 0.735$ m. A single realization of the hydraulic conductivity field is shown in Fig. 2, where lower K values are represented by lighter shades and higher K values are represented by darker shades.

For each hydraulic conductivity field generated, the associated variable hydraulic head field and groundwater velocity field are determined. The variable hydraulic head field is evaluated numerically by solving the following steady state two-dimensional groundwater flow equation for a heterogeneous confined aquifer (Bear, 1979):

$$\frac{\partial}{\partial x}\left[K(x,z)\frac{\partial h(x,z)}{\partial x}\right] + \frac{\partial}{\partial z}\left[K(x,z)\frac{\partial h(x,z)}{\partial z}\right] = 0 \quad , \tag{9}$$

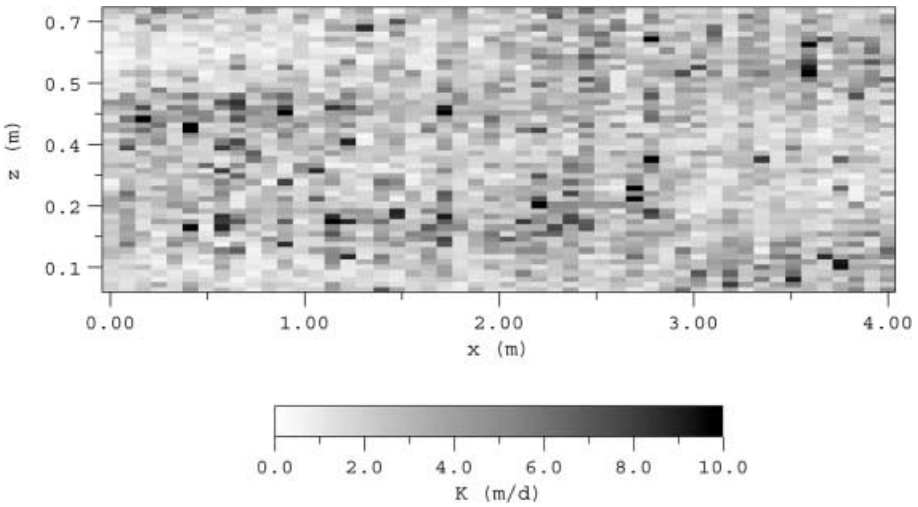

Fig. 2. Illustration of a single realization of the statistically anisotropic hydraulic conductivity field. The gray scale represents magnitude of the hydraulic conductivity (here $\zeta_x = 0.5$ m, $\zeta_z = 0.05$ m, $\bar{Y} = 0.8$, $\sigma_Y^2 = 0.3$)

where $h(x, z)$ is the hydraulic head, which is equal to total head potential.

The appropriate groundwater flow boundary conditions are

$$h(t, 0, z) = h_0 \quad , \tag{10}$$

$$h(t, L, z) = h_L \quad , \tag{11}$$

$$\frac{\partial h(t, x, 0)}{\partial z} = 0 \quad , \tag{12}$$

$$\frac{\partial h(t, x, H)}{\partial z} = 0 \quad . \tag{13}$$

Boundary conditions (10) and (11) fix the overall hydraulic gradient across the model domain. Impermeable boundaries corresponding to impermeable bedrock and an impermeable confining layer are represented by zero flux boundary conditions (12) and (13), respectively. Interstitial groundwater flow velocities, used in the governing transport equation (1), are determined using the hydraulic head distribution given by (9) and the following equations:

$$U_x(x, z) = -\frac{K(x, z)}{\theta} \frac{\partial h(x, z)}{\partial x} \quad , \tag{14}$$

$$U_z(x, z) = -\frac{K(x, z)}{\theta} \frac{\partial h(x, z)}{\partial z} \quad , \tag{15}$$

where θ is the effective porosity of the porous medium. The porosity is assumed constant even though the hydraulic conductivity field is variable. Variability in porosity is assumed to be insignificant compared to the variability in hydraulic conductivity, therefore it will not substantially affect steady state flow (Freeze, 1975; Dagan, 1989).

2.3
Model parameters

The aqueous phase molecular diffusion coefficient for 1,1,2-TCA, at 25 °C obtained using the Hayduk and Laudie relationship, is $\mathscr{D} = 1.6 \times 10^{-6}$ m^2/h (Hayduk and Laudie, 1974; Lee and Chrysikopoulos, 1998). Employing a tortuosity value of $\tau^* = 1.43$ for clean sand (de Marsily, 1986), the calculated effective diffusion coefficient for 1,1,2-TCA is $\mathscr{D}_e = 2.33 \times 10^{-6}$ m^2/h.

Spatially variant hydrodynamic dispersion coefficients are calculated using the following relationships (Bear, 1979):

$$D_x(x,z) = \frac{\alpha_T U_z^2(x,z) + \alpha_L U_x^2(x,z)}{|\mathbf{U}|} + \mathscr{D}_e \ , \tag{16}$$

$$D_z(x,z) = \frac{\alpha_T U_x^2(x,z) + \alpha_L U_z^2(x,z)}{|\mathbf{U}|} + \mathscr{D}_e \ , \tag{17}$$

where

$$|\mathbf{U}| = [U_x^2(x,z) + U_z^2(x,z)]^{1/2} \ , \tag{18}$$

is the magnitude of the interstitial velocity vector; and α_L and α_T are the longitudinal and transverse dispersivities, respectively.

Assuming instantaneous, reversible, and linear sorption, the retardation factor in the aquifer is defined by (Hashimoto et al., 1964);

$$R = 1 + \frac{\rho_b}{\theta} K_d \ , \tag{19}$$

where ρ_b is the bulk density of the solid matrix; $K_d = f_{oc} K_{oc}$ is the partition coefficient where f_{oc} is the fraction of organic carbon in the porous medium and K_{oc} is the octanol-water partition coefficient (Karickhoff, 1984). In this work, values used for f_{oc} and K_{oc} are 0.16% and 7.0×10^{-5} m^3/g, respectively (Mackay et al., 1992). Assuming an aquifer bulk density of 1.69×10^6 g/m^3 and an effective porosity of 0.3, the retardation factor for 1,1,2-TCA is estimated to be $R = 1.63$.

Local time dependent mass transfer coefficient values along the length of the DNAPL pool are determined by rearranging (5) and solving for $k(t,x)$. The average mass transfer coefficient is given by

$$\bar{k}(t) = \frac{1}{\ell_x N} \sum_{i=1}^{N} \int_{\ell_{x_0}}^{\ell_{x_0}+\ell_x} k_i(t,x) \mathrm{d}x \ , \tag{20}$$

where N is the number of different log-normally distributed hydraulic conductivity field realizations examined. Table 1 lists all model parameter values used in this study.

3
Numerical modeling

The two-dimensional mathematical model for contaminant transport and groundwater flow is solved numerically by a finite difference approximation. For

Table 1. Parameter values for numerical simulations

Parameter	Parameter value
C_b	0.0 g/l
C_s	4.5 g/l†
$\mathscr{D}_e$	2.33×10^{-6} m^2/h†
d	0.003 m
H	0.735 m
ℓ_x	0.72 m
ℓ_{x_0}	0.64 m
L	3.92 m
R	1.63†
$\bar{Y}$	0.8, 0.9
α_L	3.3×10^{-2} m
α_T	3.3×10^{-3} m
Δt	1 h
ζ_x	0.50 m
ζ_z	0.03–0.50 m
θ	0.3
σ_Y^2	0.1–0.5
τ^*	1.43

†Data for 1,1,2-TCA

the contaminant transport model, a zero dispersive flux boundary condition is applied to all outer boundaries of the numerical domain with the exception of the DNAPL pool. Concentrations at nodes along the DNAPL pool are kept constant at the 1,1,2-TCA solubility limit C_s. For the groundwater model, constant head boundaries are used on the left and right of the numerical domain to attain steady state flow. The top and bottom boundaries, corresponding to the confining layer and impermeable bedrock, respectively, are defined by no-flux boundary conditions. The physical model domain together with the appropriate boundary conditions are schematically illustrated in Fig. 1.

3.1
Groundwater flow solution

The steady state groundwater flow equation (9), subject to boundary conditions (10)–(13), is solved numerically using an implicit finite difference scheme with node spacing $\Delta x = 0.08$ m and $\Delta z = 0.015$ m in the x and z directions, respectively. The left and right constant head boundary conditions are given by (10) and (11), respectively. Zero flux boundary conditions (12) and (13), corresponding to the lower and upper impermeable layers, respectively, are solved numerically by the method of images. Equation (9) is solved at every node of the 50×50 node grid. The resulting matrix is band diagonal and represents a system of equations that can be efficiently solved using the numerical subroutines *bandec* and *banbks* (Press et al., 1992). Using the estimated hydraulic head distribution, the spatially variant interstitial groundwater velocity is then determined by (14) and (15).

3.2
Contaminant transport solution

The contaminant transport of aqueous phase solute described by (1) is solved using the backwards in time alternating direction implicit (ADI) finite difference scheme. In the ADI method, concentration is first solved along columns implicitly, then along rows explicitly. One complete solution sweep involves solving for

concentration over half of a time step, $\Delta t/2$, for each individual sweep along columns then rows, resulting in an unconditionally stable algorithm. A time step of $\Delta t = 1$ h was used in all simulations. Solving only one-dimension at a time, either along rows or columns, results in a system of equations forming a tridiagonal matrix. The tridiagonal matrix may be efficiently solved using the Thomas algorithm. For each realization of the hydraulic conductivity field, local mass transfer coefficients were determined from (5) at each node at the NAPL-water interface by using the second-order accurate one-sided approximation of the concentration gradient above the NAPL pool (Strikwerda, 1989). The local mass transfer coefficients were averaged over the length of the NAPL pool and the average (or overall) mass transfer coefficient was determined from (20) by averaging the results from 200 realizations of the hydraulic conductivity field.

3.3
Comparison with an analytical solution

The numerical finite difference solution to the contaminant transport problem (1)–(6), is compared to the two-dimensional analytical solution derived by Chrysikopoulos et al. (1994)

$$\frac{C}{C_s} = \frac{\mathrm{Sh_o}}{2}\int_0^T \left(\frac{1}{\pi \mathrm{Pe}_z R\tau}\right)^{1/2} \exp\left[-\Lambda\tau - \frac{\mathrm{Pe}_z R Z^2}{4\tau}\right] \left\{ \mathrm{erf}\left[\left(X - \frac{\tau}{R}\right)\left(\frac{\mathrm{Pe}_x R}{4\tau}\right)^{1/2}\right] - \mathrm{erf}\left[\left(X - 1 - \frac{\tau}{R}\right)\left(\frac{\mathrm{Pe}_x R}{4\tau}\right)^{1/2}\right]\right\} \mathrm{d}\tau, \tag{21}$$

where $\mathrm{Pe} = U_x \ell_x / \mathscr{D}_e$ is the Péclet number; $\mathrm{Sh_o} = \bar{k}\ell_x \mathscr{D}_e$ is the overall Sherwood number; $T = U_x t/\ell_x$ is dimensionless time; $X = (x - \ell_{x_0})/\ell_x$ is dimensionless distance; $\Lambda = \lambda \ell_x / U_x$ is the dimensionless decay coefficient; and τ is a dummy integration variable. For the special case of uniform longitudinal interstitial fluid and a 1,1,2-TCA pool, the numerical and analytical solutions are compared at $t = 5000$ h and the results are presented in Fig. 3. Clearly, there is very good agreement between the numerical and analytical solutions, indicating that the numerical scheme employed in the present work is relatively accurate.

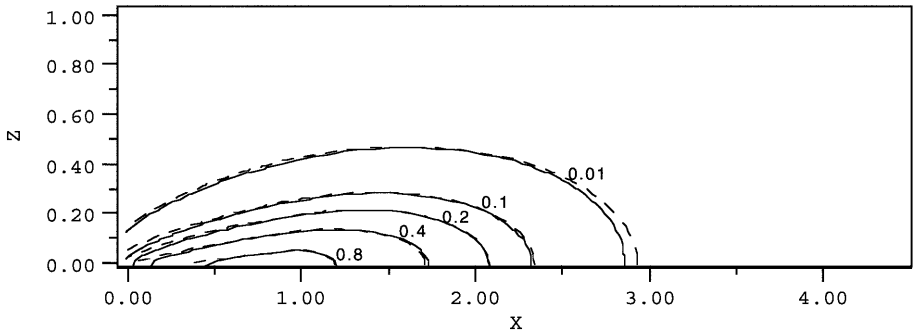

Fig. 3. Comparison between normalized 1,1,2-TCA dissolved concentration contours predicted by the Chrysikopoulos et al. (1994) analytical solution (solid line) and the finite-difference model (dashed line) at $t = 5000$ h (here $\ell_{x_0} = 0.64$ m, $\ell_x = 0.72$ m, $\bar{k} = 0.28 \times 10^{-4}$ m/hr, $U_x = 0.325 \times 10^{-3}$ m/hr)

4
Simulations and discussion

Several numerical simulations were performed in order to investigate the effects of the various model parameters on the DNAPL pool dissolution. The groundwater interstitial velocity was varied by changing the hydraulic gradient $\partial h/\partial x$ in the range 0.002 to 0.01. These two hydraulic gradients represent typical hydraulic gradients for regional flow and flow near a pumping well, respectively. Two mean log-normal hydraulic conductivities, representative of a fine to course sand, ($\bar{Y} = 0.8, 0.9$) were employed. All numerical results presented are evaluated at $t = 5000$ h and represent the average of 200 different realizations of the log-normal hydraulic conductivity. Furthermore, the variance of the log-normal hydraulic conductivity field was varied from 0.1–0.5 and the correlation length scale in the z direction was varied from 0.05–0.5 m while the correlation length scale in the x direction was kept constant at 0.5 m yielding anisotropy ratios (ζ_z/ζ_x) in the range from 0.1 to 1.0.

Numerically evaluated average mass transfer coefficients $\bar{k}$ as a function of ζ_z/ζ_x for several variances of $Y = \ln K$ ($\sigma_Y^2 = 0.1, 0.2, 0.3, 0.4$, and 0.5) at two different hydraulic gradients ($\partial h/\partial x = 0.002, 0.01$) and two different mean log-transformed hydraulic conductivities ($\bar{Y} = 0.8, 0.9$) are shown in Fig. 4. The results indicate that for increasing ζ_z/ζ_x there is a significant increase in $\bar{k}$. Low values of the anisotropy ratio ζ_z/ζ_x may represent the presence of thin lenticular layers of varying hydraulic conductivity which are observed in some sedimentary rocks (Smith, 1981). Consequently, for low ζ_z/ζ_x ratios, transverse dispersion is significant causing more vertical spreading of the dissolved 1,1,2-TCA concentration plume which in turn leads to a thicker concentration boundary layer, smaller concentration gradients at the pool-water interface, and smaller $\bar{k}$ values. Increasing ζ_z/ζ_x, the hydraulic conductivity becomes progressively more statistically similar in the vertical direction. At the limit where the anisotropic ratio approaches unity, the aquifer can be described as homogeneously heterogeneous without a preferential principal direction of anisotropy. For high ζ_z/ζ_x ratios the dissolved 1,1,2-TCA concentration boundary layer is thinner because vertical dispersion is reduced across statistically similar lenticular layers yielding steeper concentration gradients at the pool-water interface and greater $\bar{k}$ values.

Comparison of Figs. 4a and b indicates that $\bar{k}$ increases with increasing hydraulic gradient or equivalently increasing interstitial velocity. It should be noted that the effect of the anisotropy ratio ζ_z/ζ_x on $\bar{k}$ is more pronounced at higher hydraulic gradients (compare Figs. 4b and d). At higher interstitial velocities concentration gradients within the boundary layer are steeper leading to greater $\bar{k}$. Figure 5 illustrates the effect of hydraulic gradient on the dissolved concentration boundary layer thickness resulting from the dissolution of a 1,1,2-TCA pool. Similar results have been observed in recent theoretical (Kim and Chrysikopoulos, 1999; Chrysikopoulos and Kim, 2000) and experimental (Chrysikopoulos et al., 2000) DNAPL pool dissolution studies.

The results presented in Fig. 4 also indicate that increasing the variance of the log-transformed hydraulic conductivity distribution leads to a decreasing average mass transfer coefficient. This is an intuitive result because by increasing σ_Y^2 the heterogeneity of the porous medium is increased, the spreading of the dissolved plume is increased in the vertical direction, and consequently, the concentration gradients at the pool-water interface are reduced leading to $\bar{k}$ reduction. The effect of σ_Y^2 on the dissolved concentration distribution within an aquifer is illustrated in Fig. 6.

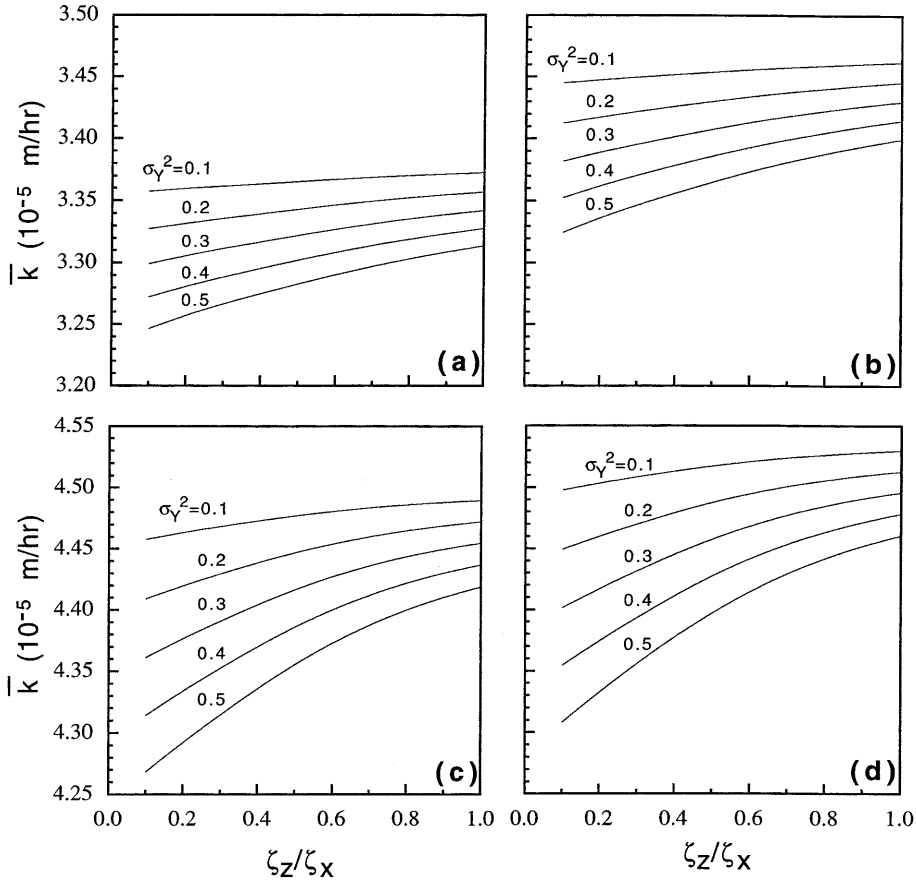

Fig. 4a–d. Average mass transfer coefficient as a function of aquifer anisotropy ratio for several variances of the log-transformed hydraulic conductivity distribution at **a** $\partial h/\partial x = 0.002$, $\bar{Y} = 0.8$; **b** $\partial h/\partial x = 0.002$, $\bar{Y} = 0.9$; **c** $\partial h/\partial x = 0.01$, $\bar{Y} = 0.8$; and **d** $\partial h/\partial x = 0.01$, $\bar{Y} = 0.9$ (here $t = 5000$ h)

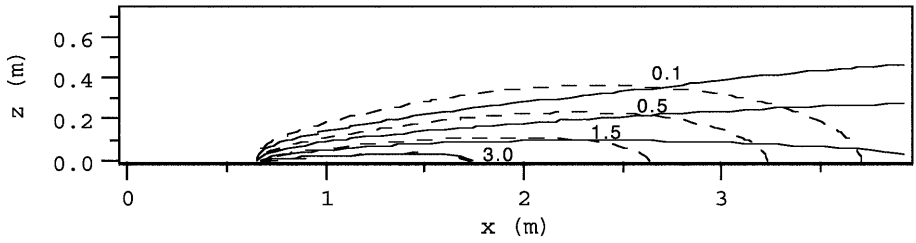

Fig. 5. Comparison between dissolved concentration contours originating from a 1,1, 2-TCA pool for $\partial h/\partial x = 0.01$ (solid line) and 0.002 (dashed line) (here $\ell_{x_0} = 0.64$ m, $\ell_x = 0.72$ m, $\zeta_x = 0.5$ m, $\zeta_z = 0.5$ m, $\bar{Y} = 0.8$, $\sigma_Y^2 = 0.5$; $t = 5000$ h)

Numerically evaluated $\bar{k}$ values as a function of σ_Y^2 for several anisotropy ratios ($\zeta_z/\zeta_x = 0.1, 0.5$, and 1.0) at two different hydraulic gradients ($\partial h/\partial x = 0.002, 0.01$) and two different mean log-transformed hydraulic conductivities ($\bar{Y} = 0.8, 0.9$) are presented in Fig. 7 together with the best fitted lines. The results

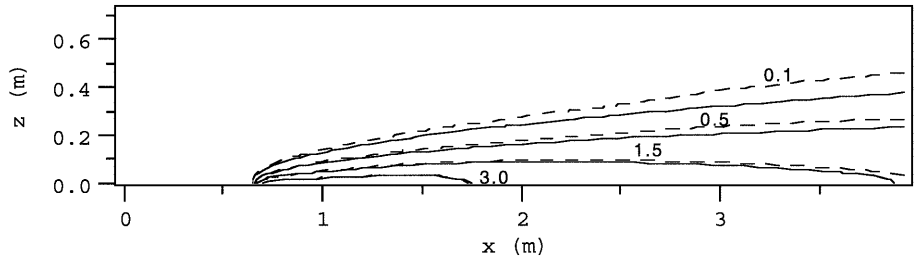

Fig. 6. Comparison between dissolved concentration contours originating from a 1,1,2-TCA pool for $\sigma_Y^2 = 0.5$ (dashed line) and 0.1 (solid line) (here $\ell_{x_0} = 0.64$ m, $\ell_x = 0.72$ m, $\partial h/\partial x = 0.01$, $\zeta_x = 0.5$ m, $\zeta_z = 0.5$ m, $\bar{Y} = 0.8$, $t = 5000$ h)

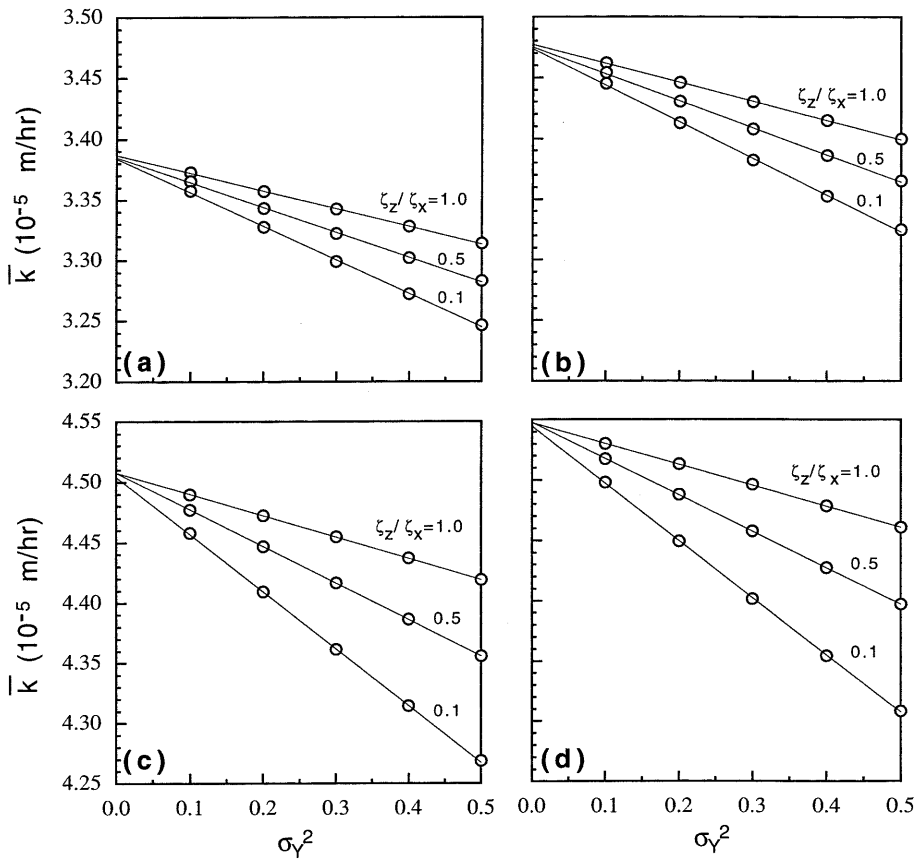

Fig. 7a-d. Average mass transfer coefficients as a function of the variance of the log-transformed hydraulic conductivity distribution for **a** $\partial h/\partial x = 0.002$, $\bar{Y} = 0.8$; **b** $\partial h/\partial x = 0.002$, $\bar{Y} = 0.9$; **c** $\partial h/\partial x = 0.01$, $\bar{Y} = 0.8$; and **d** $\partial h/\partial x = 0.01$, $\bar{Y} = 0.9$. Open circles represent numerically generated data and solid lines represent linear fits (here $t = 5000$ h)

indicate that $\bar{k}$ is inversely proportional to σ_Y^2. A strong linear relationship is observed suggesting that a correlation between $\bar{k}$ and σ_Y^2, ζ_z/ζ_x, and $\bar{Y}$ can be developed. However, such correlation is dependent on the specific DNAPL component and it is beyond the scope of the present study. Furthermore, in agreement with the results presented in Fig. 4, it is also evident from Fig. 7 that $\bar{k}$

values increase with increasing ζ_z/ζ_x and/or $\bar{Y}$. It should be noted that increasing σ_Y^2 and/or $\bar{Y}$ results in larger mean hydraulic conductivity $\bar{K}$ because (Ang and Tang, 1975).

$$\bar{K} = \exp\left[\bar{Y} + \frac{\sigma_Y^2}{2}\right] \quad . \tag{22}$$

However, increasing σ_Y^2 results in increased aquifer heterogeneity with a broader range of K values. Consequently, $\bar{k}$ is more sensitive to increasing aquifer heterogeneity due to increasing σ_Y^2 than the corresponding apparent increase in $\bar{K}$. Note that $\bar{k}$ increases with increasing $\bar{K}$ or $\bar{Y}$ (compare Figs. 7a and b) but it is shown to decrease with increasing aquifer heterogeneity (see Figs. 4 and 7).

5 Summary

In order to determine the effect of aquifer anisotropy and heterogeneity on the average mass transfer coefficient associated with DNAPL pool dissolution in saturated porous media, a numerical model was developed to simulate 1,1,2-TCA pool dissolution in two-dimensional porous media. Aquifer anisotropy was obtained by generating random hydraulic conductivity realizations assuming that the hydraulic conductivity is lognormally distributed and can be described by an anisotropic exponential covariance function. Groundwater velocity was varied by changing the hydraulic gradient as well as the mean log-transformed hydraulic conductivity. Model simulations indicated that increasing the mean log-transformed hydraulic conductivity and/or the hydraulic gradient results in an increase of the average mass transfer coefficient. Increasing aquifer anisotropy, an increase in $\bar{k}$ was observed particularly at low ζ_z/ζ_x ratios and high hydraulic gradients due to the formation of steep concentration gradients above the 1,1,2-TCA pool. Furthermore, it was shown that the average mass transfer coefficient is inversely proportional to the variance of the log-transformed hydraulic conductivity distribution.

References

Ang AH, Tang WH (1975) Probability Concepts in Engineering Planning and Design. Vol I Basic Principles, Wiley, New York

Bear J (1979) Hydraulics of Groundwater. McGraw-Hill, Inc., New York

Bear J, Verruijt A (1987) Modeling Groundwater Flow and Pollution. D. Reidel, Dordrecht, Holland, 243–244 pp

Burr DT, Sudicky EA, Naff RL (1984) Nonreactive and reactive solute transport in three-dimensional heterogeneous porous media: Mean displacement, plume spreading, and uncertainty. Water Resour. Res., 30(3): 791–815

Christakos G (1992) Random Field Models in Earth Sciences. Academic Press, San Diego, California

Chrysikopoulos CV (1995a) Three-dimensional analytical models of contaminant transport from nonaqueous phase liquid pool dissolution in saturated subsurface formations. Water Resour. Res., 31(4): 1137–1145

Chrysikopoulos CV (1995b) Effective parameters for flow in saturated heterogeneous porous media. J. Hydrol., 170: 181–197

Chrysikopoulos CV, Kim T-J (2000) Local mass transfer correlations for nonaqueous phase liquid pool dissolution in saturated porous media. Transport in Porous Media, 38(1–2): 167–187

Chrysikopoulos CV, Lee KY (1998) Contaminant transport resulting from multicomponent nonaqueous phase liquid pool dissolution in three-dimensional subsurface formations. J. Contam. Hydr., 31(1–2): 1–21

Chrysikopoulos CV, Voudrias EA, Fyrillas MM (1994) Modeling of contaminant transport resulting from dissolution of nonaqueous phase liquid pools in saturated porous media. Transp. in Porous Media, 16(2): 125–145
Chrysikopoulos CV, Lee KY, Harmon TC (2000) Dissolution of a well-defined trichloroethylene pool in saturated porous media: Experimental Design and aquifer characterization. Water Resour. Res., 36(7): 1687–1696
Dagan G (1989) Flow and transport in porous formations. Springer Verlag, New York
de Marsily G (1986) Quantitative Hydrogeology: Groundwater Hydrology for Engineers. Academic Press, San Diego, California
Freeze RA (1975) A stochastic-conceptual analysis of one-dimensional groundwater flow in nonuniform homogeneous media. Water Resour. Res., 11(5): 725–741
Gelhar LW, Axness CL (1983) Three-dimensional stochastic analysis of macrodisisperion in aquifers. Water Resour. Res., 19(1): 161–180
Gutjhar AL (1989) Fast Fourier transform for random field generation, Proj. Rep. Contract No. 4-R58-2690R, for Los Alamos Grant, New Mexico Institute of Mining and Technology, Socorro, New Mexico
Hashimoto I, Deshpande KB, Thomas HC (1964) Peclet numbers and retardation factors for ion exchange columns. Industrial Engrg. Chem. Fundamentals, 3(3): 213–218
Hayduk W, Laudie H (1974) Prediction of diffusion coefficients for nonelectrolytes in dilute aqueous solutions. AIChE J., 20(3): 611–615
Incropera FP, DeWitt DP (1990) Fundamentals of Heat and Mass Transfer. 3rd edn., Wiley, New York, 919 pp
Johnson RL, Pankow JF (1992) Dissolution of dense chlorinated solvents into groundwater, 2, source functions for pools of solvent. Env. Sci. Technol., 226(5): 896–901
Khachikian C, Harmon TC (2000) Nonaqueous phase liquid dissolution in porous media: Current state of knowledge and research needs. Transport in Porous Media, 38(1–2): 3–28
Karickhoff SW (1984) Organic pollutant sorption in aquatic systems. J. Hydr. Engrg., ASCE, 110(6): 707–735
Kim T, Chrysikopoulos CV (1999) Mass transfer correlations for nonaqueous phase liquid pool dissolution in saturated porous media. Water Resour. Res., 35(2): 449–459
Kueper BH, Abbott W, Farquhar G (1989) Experimental observations of multiphase flow in heterogeneous porous media. J. Contam. Hydrol., 5: 83–85
Kueper BH, Frind EO (1991) Two-phase flow in heterogeneous porous media, 1: Model development. Water Resour. Res., 27(6): 1049–1057
Kueper BH, Frind EO (1991) Two-phase flow in heterogeneous porous media, 2: Model application. Water Resour. Res., 27(6): 1059–1070
Lee KY, Chrysikopoulos CV (1995) Numerical modeling of three-dimensional contaminant migration from dissolution of multicomponent NAPL pools in saturated porous media. Environ. Geol., 26: 157–165
Lee KY, Chrysikopoulos CV (1998) NAPL pool dissolution in stratified and anisotropic porous formations. J. Env. Eng., 124(9): 851–862
Mackay D, Shiu WY, Ma KC (1992) Illustrated Handbook of Physical-Chemical Properties and Environmental Fate for Organic Chemicals. Vol. 33, Volatile Organic Chemicals, Lewis Publishers, Chelsea, Michigan
Manivannan I, Powers SE, Curry GW Jr. (1996) Dissolution of NAPLs entrapped in hetdrogeneous porous media, in Non-Aqueous Phase Liquids (NAPLs) in Subsurface Environment: Assessment and Remediation, Reddi LN ed., American Society of Civil Engineers, New York, 563–574 pp
Mason AR, Kueper BH (1996) Numerical simulation of surfactant-enhanced solubilization of pooled DNAPL. Env. Sci. Technol., 30: 3205–3215
Mayer AS, Miller CT (1996) The influence of mass transfer characteristics and porous media heterogeneity on nonaqueous phase dissolution. Water Resour. Res., 32(6): 1551–1567
Powers SE, Nambi IM, Curry GW Jr. (1998) Non-aqueous phase liquid dissolution in heterogeneous systems: Mechanisms and a local equilibrium modeling approach. Water Resour. Res., 34(12): 3293–3302
Press WH, Flannery BP, Teukolsky SA, Vetterling WT (1992) Numerical Recipes: The Art of Scientific Computing. 2nd edn., Cambridge University Press, New York
Rivett MO, Feenstra S, Cherry JA (1994) Transport of a dissolved phase plume from a residual solvent source in a sand aquifer. J. Hydrol., 159(1–4): 27–41

Russo D, Zaidel J, Laufer A (1994) Stochatic analysis of solute transport in partially saturated heterogeneous soils, 1, Numerical experiments. Water Resour. Res., 30(3): 769–779
Smith L (1981) Spatial variability of flow parameters in a stratified sand. Math. Geol., 13(1): 1–21
Strikwerda JC (1989) Finite Difference Schemes and Partial Differential Equations, Pacific Grove, Wadsworth & Brooks/Cole, California
Sudicky EA (1986) A natural gradient experiment on solute transport in a sand aquifer: Spatial variability of hydraulic conductivity and its role in the disperion process. Water Resour. Res., 22(13): 2069–2082
Tatalovich ME, Lee KY, Chrysikopoulos CV (2000) Modeling the transport of contaminants originating from the dissolution of DNAPL pools in aquifers in the presence of dissolved humic substances. Transport in Porous Media, 38(1–2): 93–115
Whelan MP, Voudrias EA, Pearce A (1994) DNAPL pool dissolution in saturated porous media: Procedure development and preliminary results. J. Contam. Hydrol., 15(3): 223–237